

Supporting Information for

Inorg. Chem.

Two Isostructural Coordination Polymers Showing Diverse Magnetic Behaviors: Weak Coupling (Ni^{II}) and an Ordered Array of Single-Chain Magnets (Co^{II})

Min Chen,[†] Hui Zhao,[†] E. Carolina Sañudo,[‡] Chun-Sen Liu^{*,†} and Miao Du^{*,†,§}

[†] Henan Provincial Key Lab of Surface & Interface Science, Zhengzhou 450002, Henan, Peoples' Republic of China

[‡] Departament de Química Inorgànica i Institut de Nanociència i Nanotecnologia, Universitat de Barcelona, Diagonal 645, 08028 Barcelona, Spain

[§] College of Chemistry, Tianjin Key Laboratory of Structure and Performance for Functional Molecules, MOE Key Laboratory of Inorganic–Organic Hybrid Functional Material Chemistry, Tianjin Normal University, Tianjin 300387, Peoples' Republic of China

^{*} E-mails: chunsenliu@zzuli.edu.cn; dumiao@public.tpt.tj.cn

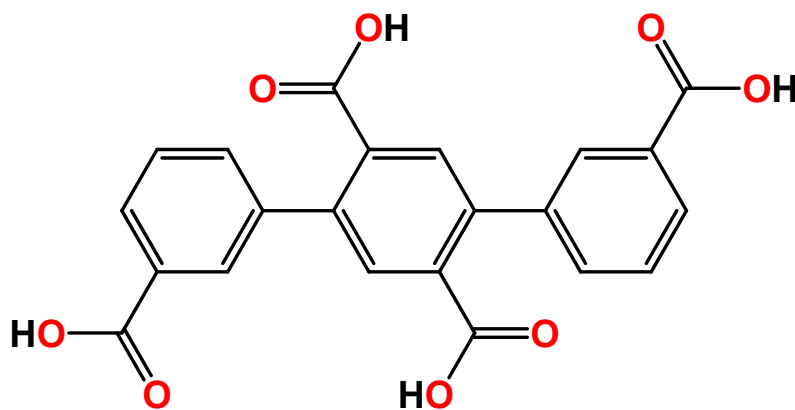
General Materials and Methods.

All of the starting reagents and solvents were obtained commercially and used as received. Elemental analysis of C, H, and N was performed on a Vario EL III Elementar analyzer. IR spectrum was measured on a Bruker Tensor 27 OPUS FT-IR spectrometer (KBr pellet) in 4000–400 cm^{-1} range. Powder X-ray diffraction (PXRD) patterns were recorded on a Rigaku (model Ultima IV) diffractometer with a Rigaku D/teX ultrahigh-speed position sensitive detector and Cu-K α X-ray (40 kV, 40mA). The powder samples were prepared by crushing the single crystals and the intensity data were taken in the step-scan mode with the scan rate of 2 $^{\circ}/\text{min}$ and step size of 0.02 $^{\circ}$. Simulation of the PXRD patterns was performed by diffraction-crystal module of the *Mercury* program using the single-crystal data. Thermogravimetric analysis (TGA) curves were taken on a Perkin-Elmer Diamond SII thermal analyzer from room temperature to 800 $^{\circ}\text{C}$, with a heating rate of 10 $^{\circ}\text{C min}^{-1}$ under N_2 atmosphere. Magnetic measurements were carried out in the Unitat de Mesures Magnètiques (Universitat de Barcelona) on polycrystalline samples (*circa* 30 mg) with a Quantum Design SQUID MPMS-XL magnetometer equipped with a 5 T magnet. Diamagnetic corrections were calculated using Pascal's constants and an experimental correction for the sample holder was applied.

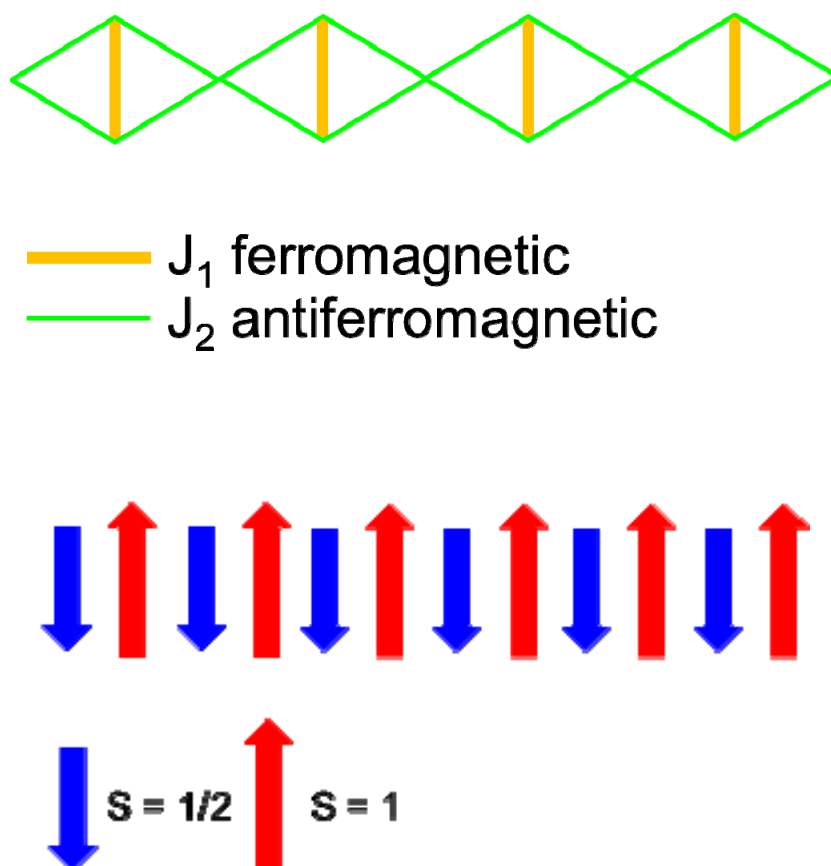
Synthesis and Characterization.

Preparation of $[\text{Ni}_3(\text{TPTA})(\text{OH})_2(\text{H}_2\text{O})_4]_n$ (1). A mixture of $\text{Ni}(\text{NO}_3)_2 \cdot 6\text{H}_2\text{O}$ (72.7 mg, 0.25 mmol), and H_4TPTA (20.3 mg, 0.05 mmol) in H_2O (8 mL) was sealed in a Teflon-lined stainless steel container and heated at 160 °C for 3 days. After cooling to room temperature, green block crystals of $1(\text{Ni}^{\text{II}})$ were obtained. Yield: 22.3 mg (65 % based on H_4TPTA). Anal. calcd for $\text{C}_{22}\text{H}_{20}\text{O}_{14}\text{Ni}_3$: C, 38.60; H, 2.95%. Found: C, 38.21; H, 2.79%. IR (KBr pellet, cm^{-1}): 3566 (s), 2999 (m, br), 1566 (s), 1393 (s), 1268 (m), 1086 (w), 903 (w), 838 (w), 772 (s), 698 (m), 611 (m), 573 (m).

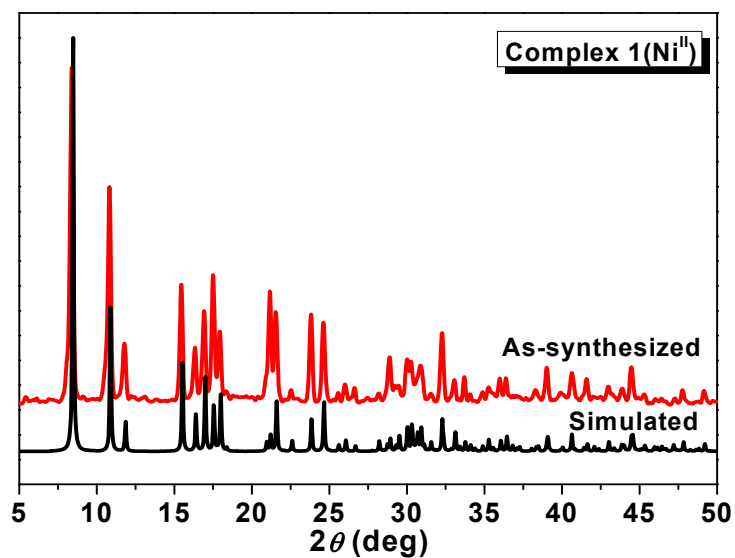
Preparation of $[\text{Co}_3(\text{TPTA})(\text{OH})_2(\text{H}_2\text{O})_4]_n$ (2). Complex $2(\text{Co}^{\text{II}})$ was obtained by the same procedure used for preparation of $1(\text{Ni}^{\text{II}})$ except that the metal salt was replaced by $\text{Co}(\text{NO}_3)_2 \cdot 6\text{H}_2\text{O}$ (72.8 mg, 0.25 mmol). Pink block crystals of $2(\text{Co}^{\text{II}})$ were obtained. Yield: 20.6 mg (60% based on H_4TPTA). Anal. calcd for $\text{C}_{22}\text{H}_{20}\text{O}_{14}\text{Co}_3$: C, 38.56; H, 2.94%. Found: C, 38.18; H, 2.71%. IR (KBr pellet, cm^{-1}): 3569 (m), 2998 (m, br), 1571 (s), 1396 (s), 1269 (m), 1086 (w), 906 (w), 840 (w), 776 (s), 700 (m), 614 (m), 578 (m).



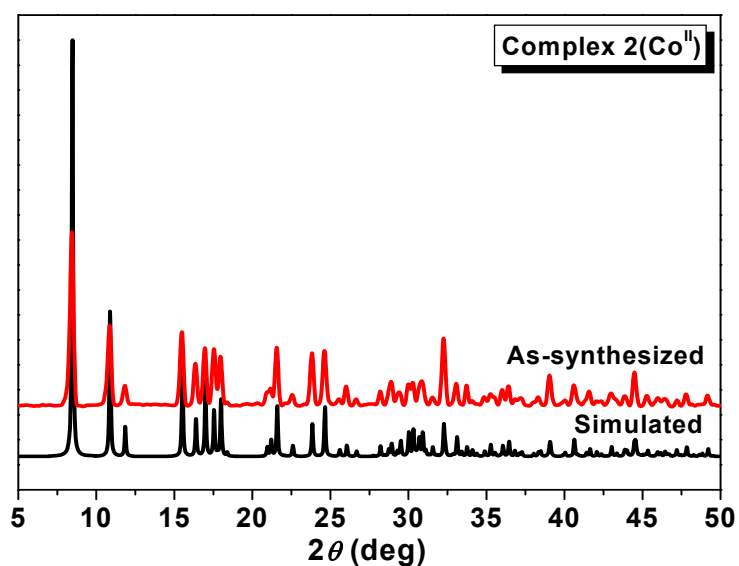
Scheme S1. Schematic drawing of the ligand H_4TPTA .



Scheme S2. Cartoon of the spin structure of the chains for $2(\text{Co}^{\text{II}})$.



(a)



(b)

Figure S1. Power X-ray diffraction patterns for (a) **1**(Ni^{II}) and (b) **2**(Co^{II}). Although the experimental pattern shows a few unindexed diffraction lines and some diffraction lines are slightly broadened in comparison with those simulated from the single crystal modes, it still can be considered favorably that the bulk synthesized materials and the as-grown crystals are homogeneous for **1** and **2**.

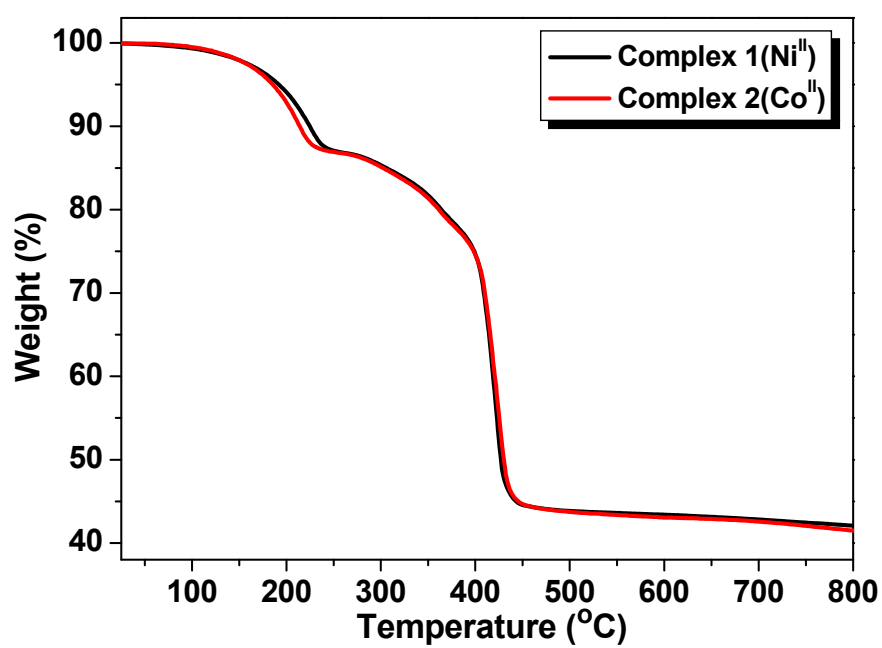


Figure S2. TGA curves of **1**(Ni^{II}) and **2**(Co^{II}).

Single-Crystal X-Ray Crystallography.

Single-crystal X-ray diffraction data for complexes **1**(Ni^{II}) and **2**(Co^{II}) were collected on an Oxford Xcalibur Gemini Eos diffractometer using graphite-monochromated Mo-K α radiation ($\lambda = 0.71073$ Å) at 294(2) K. Multi-scan absorption corrections were performed with the *CrysAlisPro* program.^{S1} Empirical absorption corrections were carried out by using spherical harmonics, implemented in *SCALE3 ABSPACK* scaling algorithm. The structure was solved by direct methods, and all non-hydrogen atoms were refined anisotropically by full-matrix least-squares method with the SHELXTL crystallographic software package.^{S2} All hydrogen atoms were generated geometrically and refined isotropically as riding. Notably, the crystal structure of **2**(Co^{II}) obtained under hydrothermal condition has been previously reported.^{S3} Crystallographic data and structural refinement details for **1**(Ni^{II}) and **2**(Co^{II}) were listed in Table S1. A comparison of the selected bond lengths and angles was shown in Table S2.

Table S1. Crystallographic Data and Structure Refinement Details for **1**(Ni^{II}) and **2**(Co^{II}).

	1 (Ni ^{II})	2 (Co ^{II})
Empirical formula	C ₂₂ H ₂₀ O ₁₄ Ni ₃	C ₂₂ H ₂₀ O ₁₄ Co ₃
Formula weight	684.51	685.17
Crystal system	Monoclinic	Monoclinic
Space group	<i>P</i> 2 ₁ / <i>c</i>	<i>P</i> 2 ₁ / <i>c</i>
<i>a</i> / Å	10.8352(10)	10.8637(5)
<i>b</i> / Å	6.3246(7)	6.3883(3)
<i>c</i> / Å	16.8834(17)	16.9630(9)
β / °	105.667(11)	105.757(6)
Volume / Å ³	1114.0(2)	1133.01(10)
<i>Z</i>	2	2
<i>D</i> / g cm ^{−3}	2.041	2.008
μ / mm ^{−1}	2.591	2.251
<i>F</i> (000)	696	690
<i>R</i> _{int}	0.0440	0.0350
Goodness-of-fit on <i>F</i> ²	1.007	0.999
<i>R</i> ₁ ^{<i>a</i>} / <i>wR</i> ₂ ^{<i>b</i>} [<i>I</i> > 2σ(<i>I</i>)]	0.0578 / 0.1554	0.0410 / 0.0827
<i>R</i> ₁ ^{<i>a</i>} / <i>wR</i> ₂ ^{<i>b</i>} (All data)	0.1001 / 0.1848	0.0697 / 0.0963
Residuals / e Å ^{−3}	0.584, −0.675	0.356, −0.462
CCDC number	1062750	1062751

^{*a*} $R_1 = \Sigma ||F_o| - |F_c|| / \Sigma |F_o|$. ^{*b*} $wR_2 = [\Sigma w(|F_o|^2 - |F_c|^2)^2 / \Sigma w(F_o^2)^2]^{1/2}$, where $w = 1/[\sigma^2(F_o^2) + (aP)^2 + bP]$. $P = (F_o^2 + 2F_c^2)/3$.

Table S2. A Comparison of the Selected Bond Lengths (Å) and Angles (°) for **1**(Ni^{II}) and **2**(Co^{II}).^a

1 (Ni ^{II})			
Ni(1)–O(1)#1	2.038(5)	Ni(1)–O(4)	2.045(5)
Ni(2)–O(7)	2.029(5)	Ni(2)–O(2)#2	2.070(5)
Ni(2)–O(3)	2.131(5)	Ni(2)–O(5)	2.106(5)
Ni(2)–O(6)	2.092(5)	Ni(1)–O(7)	2.040(4)
Ni(2)–O(7)#3	2.038(4)		
O(7)–Ni(1)–O(1)#1	84.36(18)	O(7)–Ni(1)–O(4)#4	84.73(18)
O(1)#1–Ni(1)–O(4)	88.5(2)	O(1)#1–Ni(1)–O(4)#4	91.5(2)
O(7)–Ni(1)–O(4)	95.27(18)	O(7)#4–Ni(1)–O(1)#1	95.64(18)
O(2)#2–Ni(2)–O(3)	169.5(2)	O(7)–Ni(2)–O(5)	175.67(18)
O(7)#3–Ni(2)–O(6)	176.53(19)	O(5)–Ni(2)–O(3)	82.4(2)
O(2)#2–Ni(2)–O(6)	84.40(19)	O(6)–Ni(2)–O(3)	87.91(18)
O(6)–Ni(2)–O(5)	88.4(2)	O(2)#2–Ni(2)–O(5)	90.2(2)
O(7)#3–Ni(2)–O(3)	92.68(17)	O(7)–Ni(2)–O(2)#2	92.59(19)
O(7)#3–Ni(2)–O(5)	95.04(19)	O(7)–Ni(2)–O(6)	95.13(19)
O(7)–Ni(2)–O(3)	95.23(18)	O(7)#3–Ni(2)–O(2)#2	95.43(18)
O(7)–Ni(2)–O(7)#3	81.42(19)		
2 (Co ^{II})			
Co(1)–O(1)#1	2.072(3)	Co(1)–O(4)	2.082(3)
Co(1)–O(7)	2.067(2)	Co(2)–O(2)#2	2.107(3)
Co(2)–O(3)	2.179(2)	Co(2)–O(5)	2.155(3)
Co(2)–O(6)	2.124(3)	Co(2)–O(7)	2.070(2)
Co(2)–O(7)#3	2.072(2)		
O(7)–Co(1)–O(1)#1	84.57(10)	O(7)–Co(1)–O(4)#4	85.18(9)
O(1)#1–Co(1)–O(4)	88.27(12)	O(1)#1–Co(1)–O(4)#4	91.73(12)
O(7)–Co(1)–O(4)	94.82(9)	O(7)#4–Co(1)–O(1)#1	95.43(10)

O(2)#2–Co(2)–O(3)	168.78(11)	O(7)–Co(2)–O(5)	174.81(10)
O(7)#3–Co(2)–O(6)	176.69(10)	O(5)–Co(2)–O(3)	81.56(10)
O(2)#2–Co(2)–O(6)	83.76(10)	O(6)–Co(2)–O(3)	88.28(10)
O(6)–Co(2)–O(5)	89.19(11)	O(2)#2–Co(2)–O(5)	90.40(11)
O(7)#3–Co(2)–O(3)	91.81(10)	O(7)–Co(2)–O(2)#2	92.91(11)
O(7)#3–Co(2)–O(5)	94.10(10)	O(7)–Co(2)–O(6)	95.15(10)
O(7)–Co(2)–O(3)	95.68(10)	O(7)#3–Co(2)–O(2)#2	96.59(10)
O(7)–Co(2)–O(7)#3	81.55(10)		

^a Symmetry code: For **1**(Ni^{II}): #1 = $-x + 1, y + 1/2, -z + 3/2$; #2 = $-x + 1, y - 1/2, -z + 3/2$; #3 = $-x + 1 - y, -z + 2$; #4 = $-x + 1, -y + 1, -z + 2$; For **2**(Co^{II}): #1 = $-x + 1, y + 1/2, -z + 3/2$; #2 = $-x + 1, y - 1/2, -z + 3/2$; #3 = $-x + 1, -y, -z + 2$; #4 = $-x + 1, -y + 1, -z + 2$.

Table S3. Comparison of the corresponding angles (°) in TPTA ligands in complexes **1**(Ni^{II}) and **2**(Co^{II}).

	Dihedral angle [Cg(I)–Cg(II)]	Dihedral angle [Cg(I)–Cg(III)]	Dihedral angle [Cg(II)–Cg(IV)]
1 (Ni ^{II})	60.9	50.5	18.8
2 (Co ^{II})	60.5	51.8	16.8

Section 4: Additional Structural Figures.

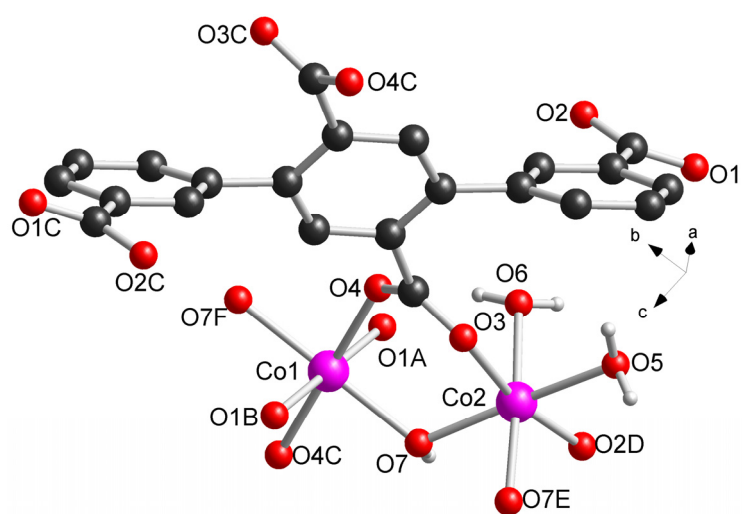


Figure S3. Coordination linkages in **2**(Co^{II}). Symmetry codes = $-x + 1, y + 1/2, -z + 3/2$ for A; $x, -y + 1/2, z + 1/2$ for B; $-x + 1, -y + 1, -z + 2$ for C; $-x + 1, y - 1/2, -z + 3/2$ for D; $-x + 2, -y + 1, -z + 2$ for G; $-x + 1, -y + 1, -z + 2$ for F; $-x + 1, -y, -z + 2$ for G.

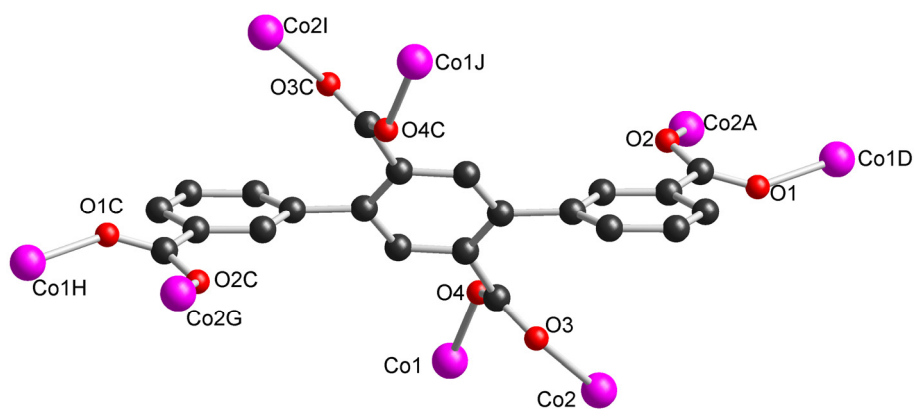


Figure S4. Coordination modes of the ligand TPTA in **2**(Co^{II}). Symmetry codes = $-x + 1, y + 1/2, -z + 3/2$ for A; $-x + 1, y - 1/2, -z + 3/2$ for D; $x + 1, -y + 1/2, z + 1/2$ for G; $-x + 2, y + 1/2, -z + 5/2$ for H; $-x + 2, -y + 1, -z + 2$ for I; $x + 1, y, z$ for J.

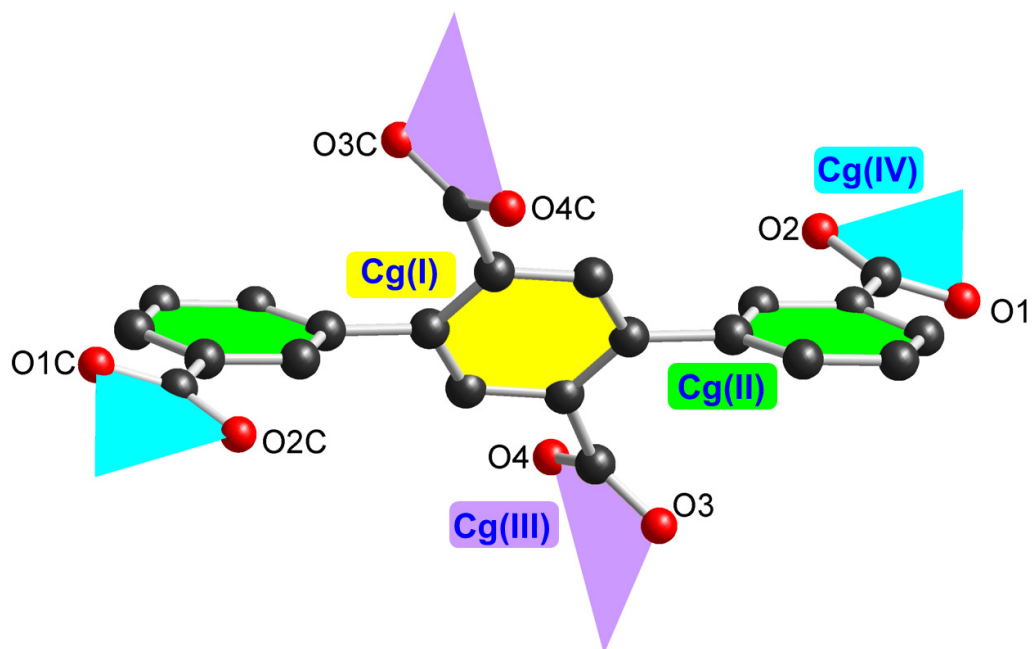


Figure S5. Arrangements of the carboxylate groups and benzene rings in **1**(Ni^{II}) and **2**(Co^{II}).

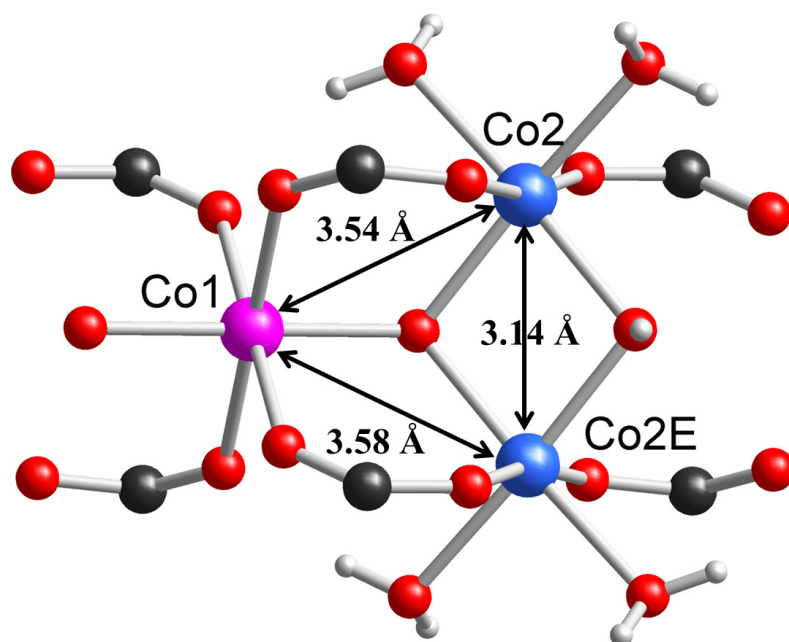


Figure S6. View of the Co···Co distances linked by the hydroxyl ligand in **2**(Co^{II}). The Co1 and Co2 centers are shown in pink and blue (symmetry code E = $-x + 1, -y, -z + 2$).

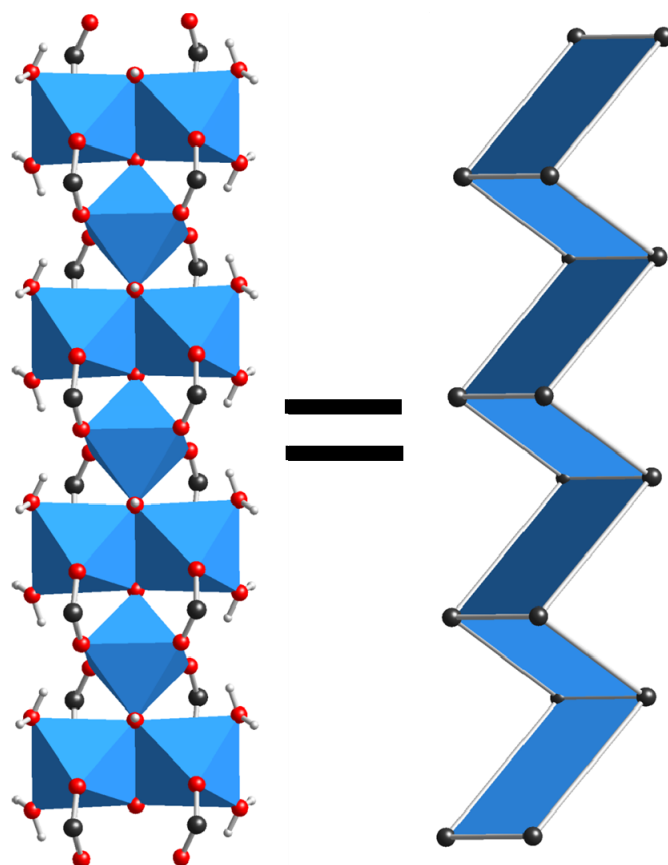


Figure S7. View of the 1-D rod-shaped SBU in **1**(Ni^{II}) and **2**(Co^{II}).

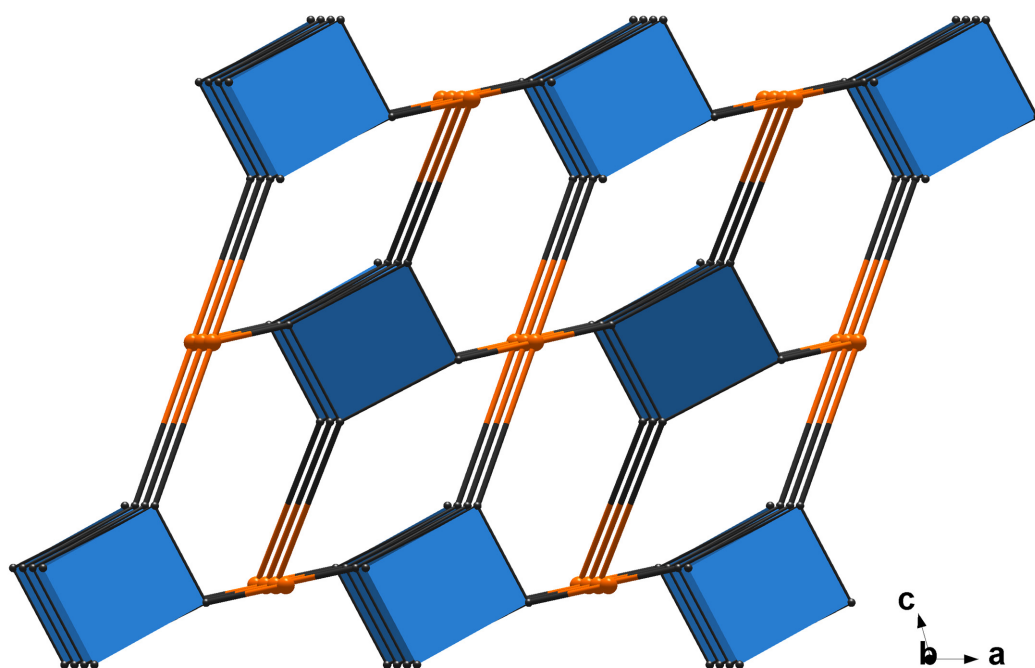


Figure S8. Schematic representation of the 3-D (4,4)-connected network in **1**(Ni^{II}) and **2**(Co^{II}).

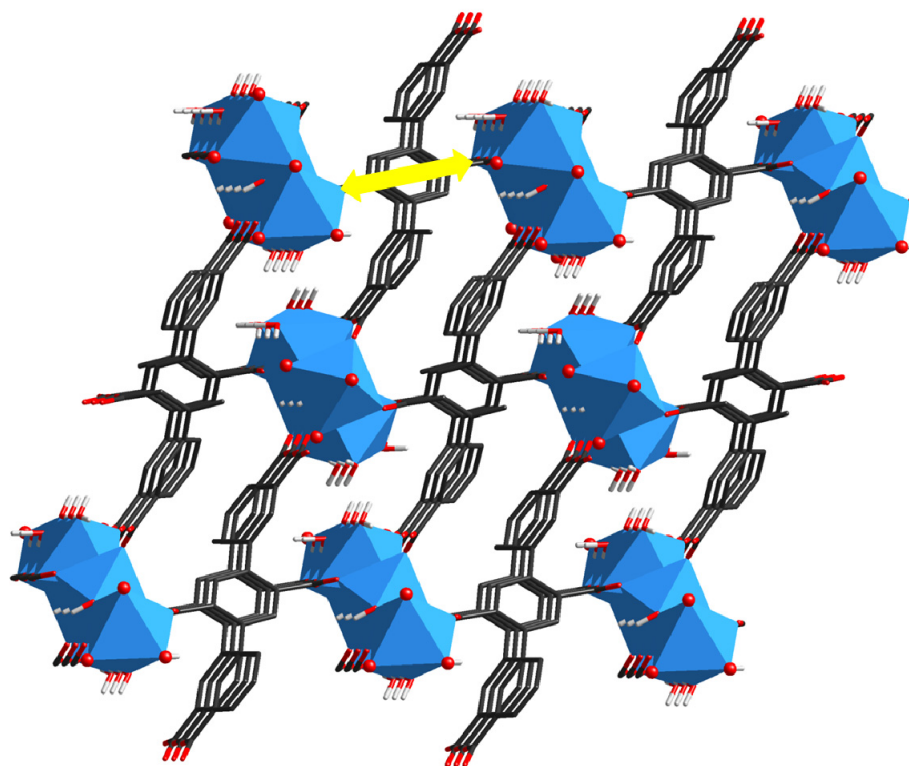


Figure S9. Crystal packing in the structure of **2**(Co^{II}) along the *b* axis, showing the shortest inter-chain exchange pathway (as a yellow arrow) through the TPTA ligand.

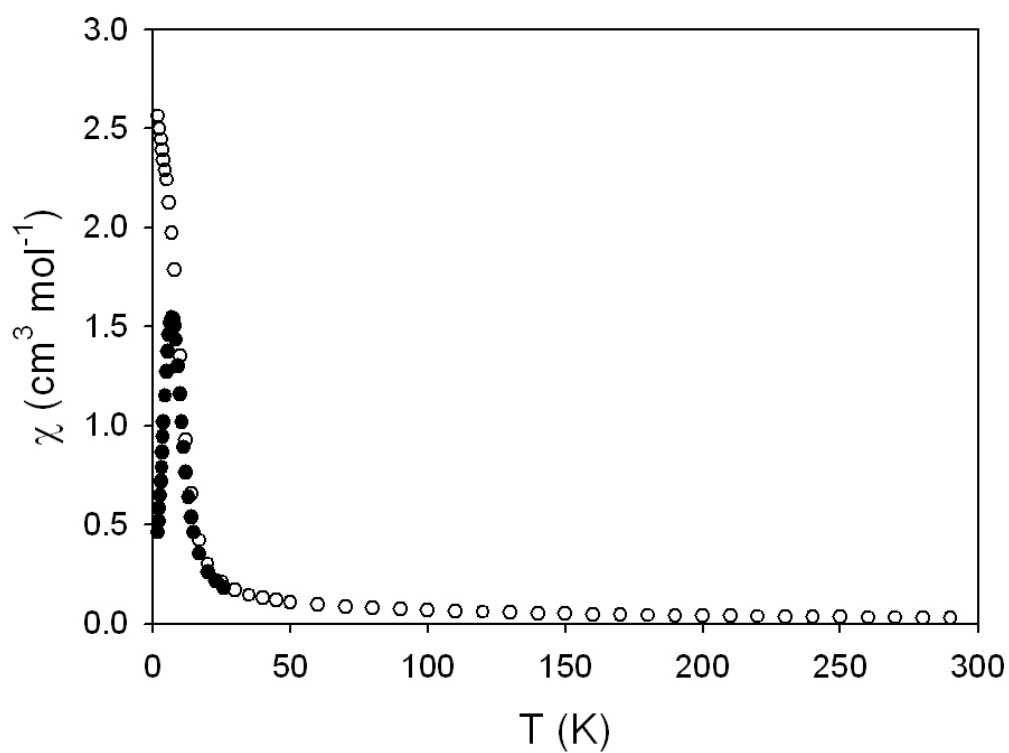


Figure S10. χ vs T plot for **2**(Co^{II}) at applied fields of 200 Oe (black circles) and 3000 Oe (white circles).

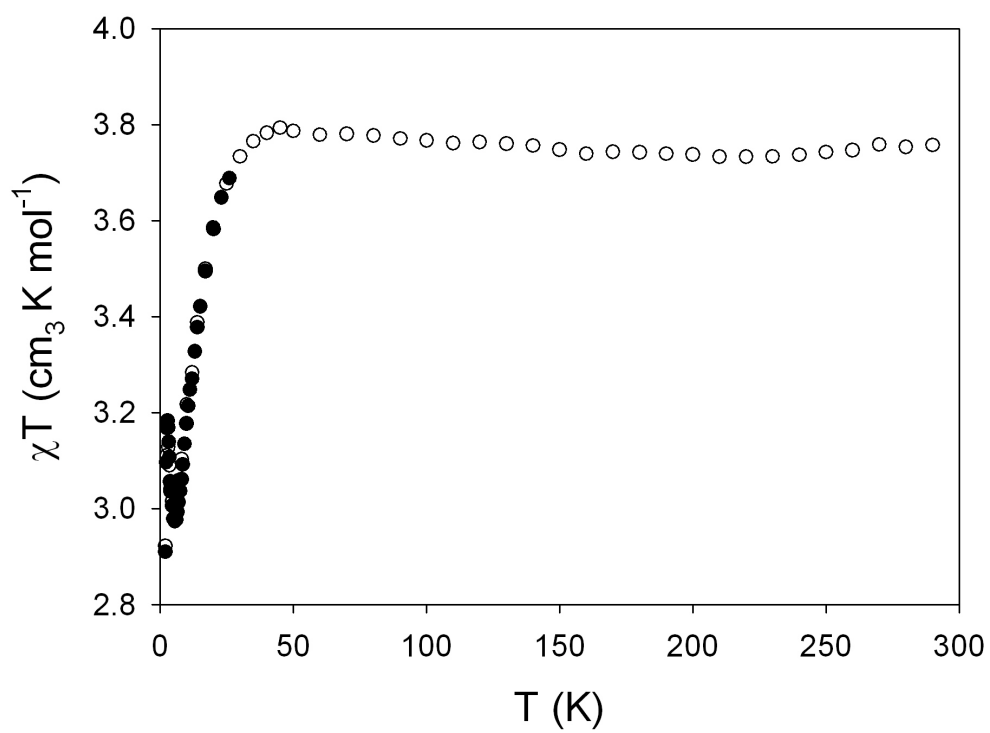


Figure S11. χT vs T plot for $\mathbf{1(Ni^{II})}$ at applied fields of 200 Oe (black circles) and 3000 Oe (white circles).

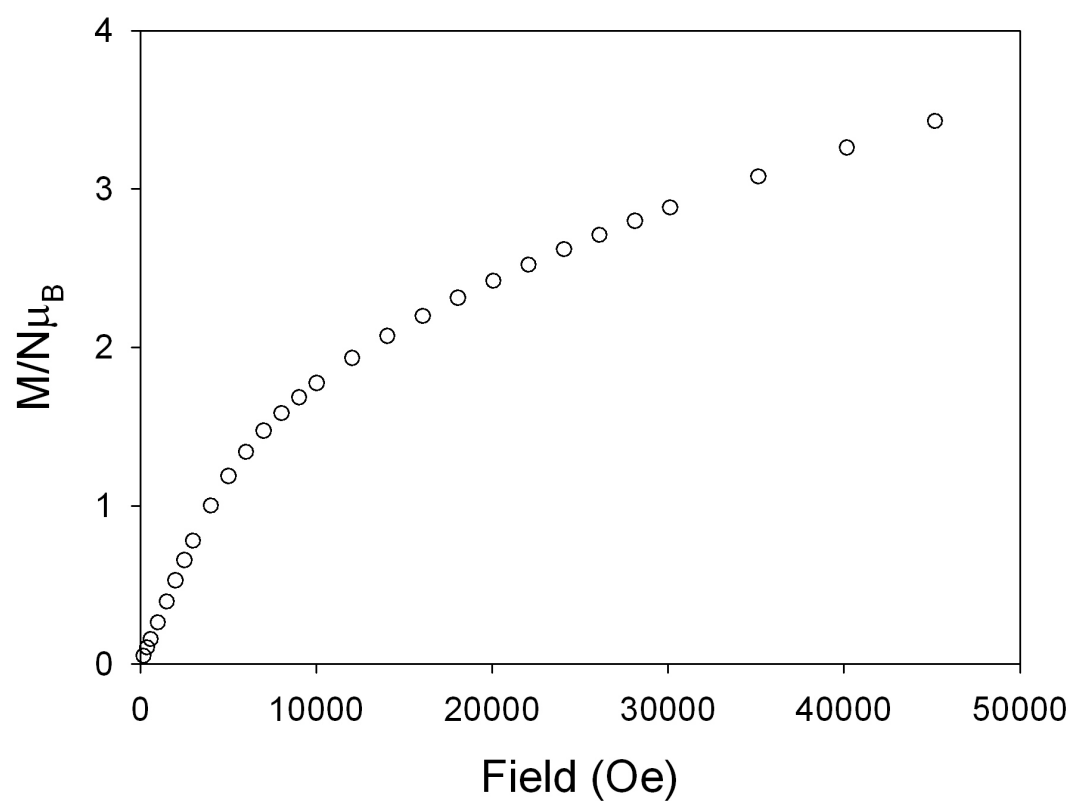


Figure S12. Magnetization vs field plot for $1(\text{Ni}^{\text{II}})$ at 2 K (white circles).

References

- (S1) *CrysAlis CCD and CrysAlis RED*, version 1.171.35.21, Oxford Diffraction Ltd: Yarnton, Oxfordshire, U. K., 2008.
- (S2) (a) Sheldrick, G. M. *SHELXTL*, version 6.10, Bruker Analytical X-ray Systems: Madison, WI, 2001;
(b) Sheldrick, G. M. *Acta Cryst.* **2008**, *A64*, 112–122.
- (S3) Ren, H.-Y.; Yao, R.-X.; Zhang, X.-M. *Inorg. Chem.* **2015**, *54*, 6312–6318.